Supplementary Information: Enhancing the Electronic-Coupling and Conductivity of Monolayer Film of Ferrocenyl Molecules by Pd and Cu Doping

Sunny M. P. Gautam,[†] Himani Malik,[†] Vikash Meghwal,[†] Sruthi Manoharan,[†] Vinithra Gurunarayanan,[†] Ramesh Ramapanicker,[†] and Thiruvancheril G. Gopakumar[*,†,‡]

[†]*Department of Chemistry, Indian Institute of Technology Kanpur, Kanpur, UP-208016, India*

[‡]*Center for Nanoscience, Indian Institute of Technology Kanpur, Kanpur, UP-208016, India.*

E-mail: gopan@iitk.ac.in

Phone: +91 5122596830

S1: Synthesis of Synthesis of (2E) (4E)-5-ferrocenyl pentadienoic acid (FcC5)

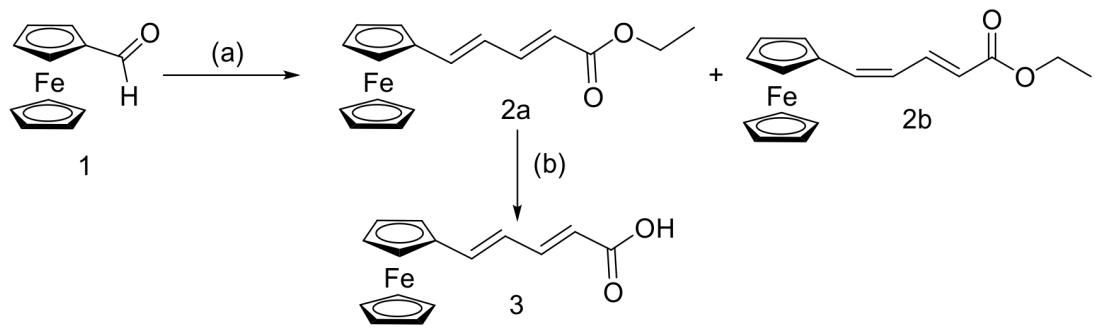

(a) KO tBu, (Ph3PCH3CH=CHCOOEt)Br, Dry THF, 0 °C - RT, 48 h
(b) LiOH, MeOH/THF (9:1), 15 h

Figure 1: Synthesis of (2E) (4E)-5-ferrocenyl pentadienoic acid.[1]

Synthesis of compound 2a

Compound 2a is synthesized as follows, to a chilled suspension of Wittig reagent ($(Ph_3CH_3CH = CHCOOEt)Br$, 2.6 mmol in 50 mL THF) potassium tert-butoxide (2.5 mmol) was added under an atmosphere of nitrogen. The resulting orange suspension was stirred at room temperature for an hour before being re-cooled to 0 °C. 1 mmol of Ferrocene carboxaldehyde (1) in 10 mL THF was then added and the suspension was stirred at 0 °C for 10 minutes. Then the mixture was allowed to warm to room temperature and stirring at room temperature for 48 hours. The mixture was diluted with 50 mL 1 M aqueous HCl and extracted with ethyl acetate. The organic extracts were combined, washed with brine, dried over Na_2SO_4, filtered, and the filtrate concentrated in vacuo to yield an orange oil. Purified by coloumn chromatography (10:90, Ethyl acetate: Pet ether) followed by recrystallisation (ethyl acetate-hexanes) yielded the title compound 2a (42% yield) as a red solid.[2]

Synthesis of compound FcC5

To a suspension of ester 2a (1 mmol) in 9:1 mL methanol: H_2O was added Lithium hydroxide (2.25 mmol). The resulting solution was stirred at room temperature for 15 hours and then acidified with $KHSO_4$ (pH $\approx$1). The resulting suspension was then extracted with ethyl acetate and the extract was combined, dried over Na_2SO_4, filtered, and the filtrate concentrated in vacuo to yield the crude title compound 3 (FcC5).

NMR data

^{1}H NMR (400 MHz, DMSO-d_6): δ 12.05 (s, 1H), 7.18 (m, 11.9 Hz, 1H), 6.81 (d, J = 15.2 Hz, 1H), 6.63-6.49 (m, 1H), 5.78 (d, J = 15.0 Hz, 1H), 4.52 (s, 2H), 4.35 (s, 2H), 4.10 (s, 5H). ^{13}C NMR (100 MHz DMSO-d_6): δ 168.21, 145.27, 140.80, 124.10, 119.01, 70.25, 69.54, 67.86.

S2: Synthesis of Synthesis of 3-ferrocenyl propenoic acid (FcC3).

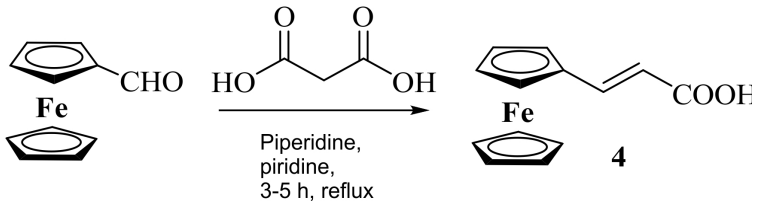

Figure 2: Synthesis of 3-ferrocenyl propenoic acid

Synthesis of FcC3

A solution of ferrocene carboxaldehyde (5 mmol), malonic acid (5 mmol), and piperidine (5 mmol) in 30 mL of pyridine was placed into a two necked round bottom flask equipped with a condenser and refluxed for 4 h under N_2 atmosphere. The crude mixture was cooled to room temperature, washed with aqueous 4 N HCl and extracted with ethyl acetate (3 * 20 mL). The organic phase was dried over anhydrous sodium sulfate, filtered and concentrated under reduced pressure to get ferrocenyl propenoic acid as red solid in 82% yield.[1]

NMR data

^{1}H NMR (400 MHz, $CDCl_3$): δ 4.18 (s, 5H); 4.45 (bs, 2H); 4.53 (bs, 2H); 6.04 (d, 1H, J = 15.6 Hz); 7.70 (d, 1H, J = 15.6 Hz). ^{13}C NMR (100 MHz, $CDCl_3$): δ 68.9; 69.8; 76.7; 78.1; 113.7; 148.6; 172.1.

S3: AFM topographs of monolayer of FcC3, FcC3-Pd and FcC3-Cu

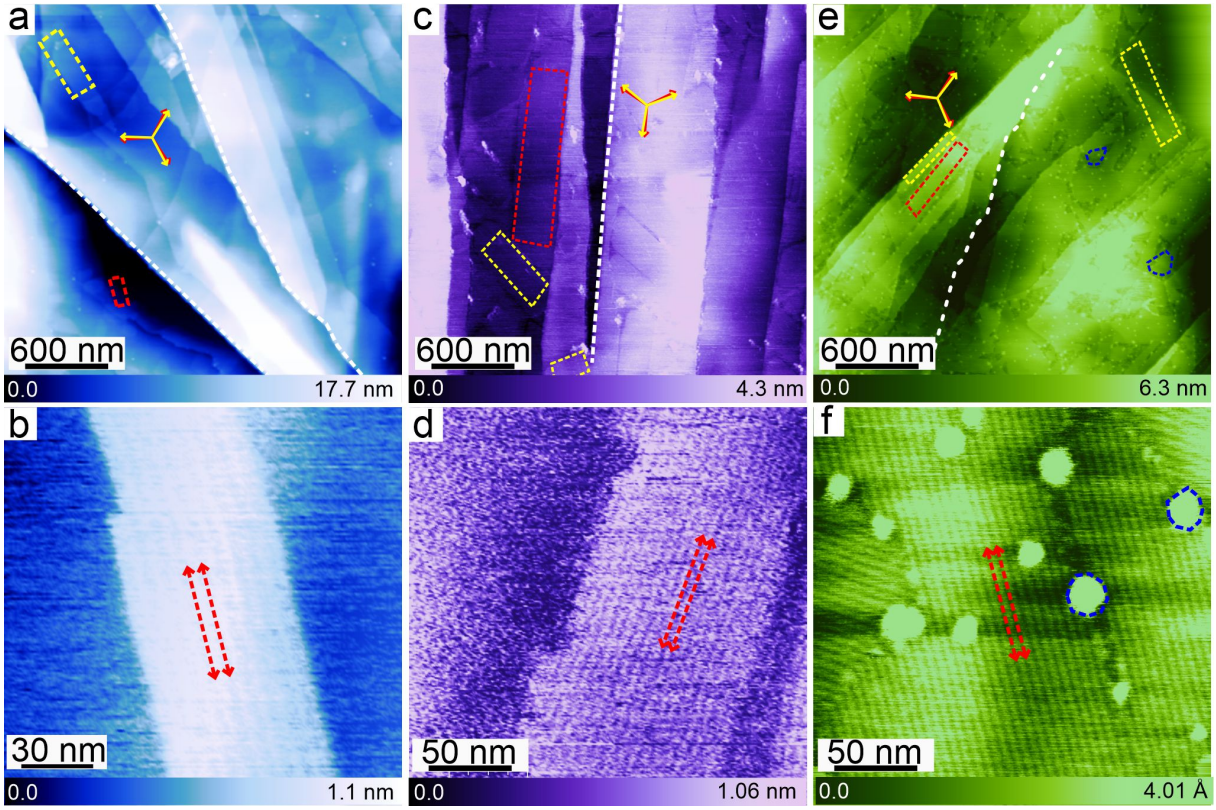

Figure 3: AFM topograph images of monolayer film of FcC3 (a,b), FcC3-Pd (c,d) and FcC3-Cu (e,f) on HOPG surface. The topographs correspond to the phase images shown in Figure 2 of manuscript. Molecular islands of FcC3, FcC3-Pd and FcC3-Cu are marked with red and yellow dashed lines. Few graphite step edges are marked with white dashed lines. Double headed arrows indicate line-like contrast running along the length of molecular islands. Blue dashed line in the film of FcC3-Cu shows additional type of islands.

S4: 2D-FFT of high resolution AFM phase images of monolayer of FcC3, FcC3-Pd and FcC3-Cu

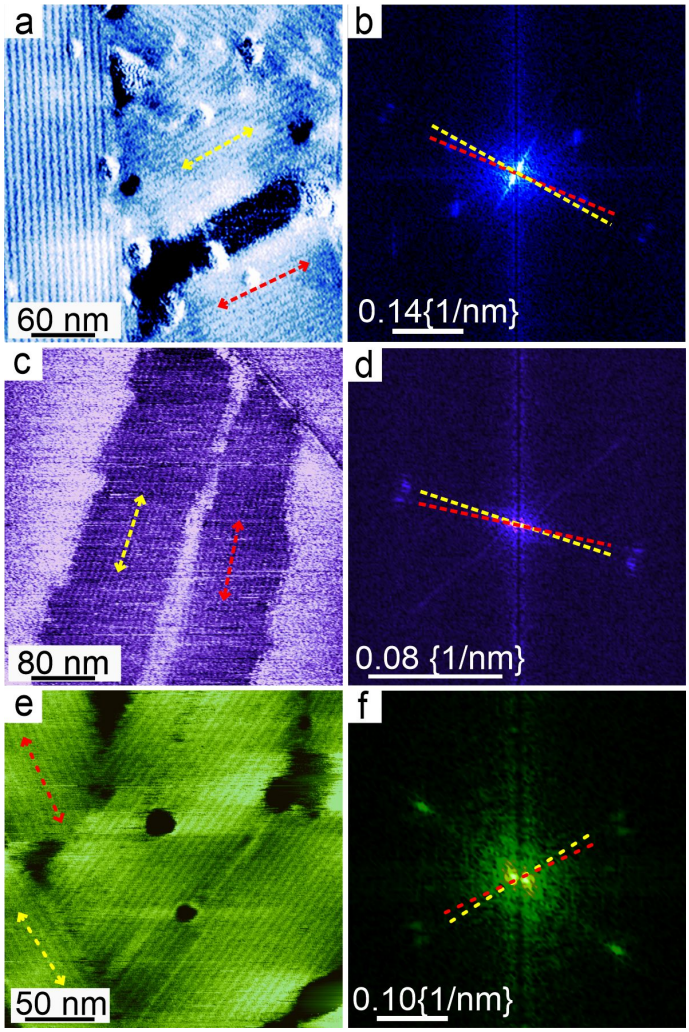

Figure 4: (a) High resolution AFM phase image of monolayer of FcC3 (a), FcC3-Pd (c) and FcC3-Cu (e) on HOPG(0001). The corresponding 2D-FFT of a, c, and e are shown in b, d, and f, respectively.

Molecular islands appear as long well defined islands. Line-like contrast is corresponds to the molecular super-lattice. The super-lattice is clearly visible in the 2D-FFT. Red and yellow arrows indicate the orientation of two domains that are mirror image to each other. This mirror image leads to the observation of six orientation for the molecular islands on surface. The mirror domains are oriented by $\approx 6\ ^{\circ}$ with respect to each other. That is

each molecular domain is rotated by $\approx 3^{\circ}$ with respect to the graphite compact directions. Note that the angle between the mirror domains are approximately same for FcC3 and FcC3-Pd/Cu films.

S5: Additonal AFM phase images of monolayer of FcC3, FcC3-Pd and FcC3-Cu

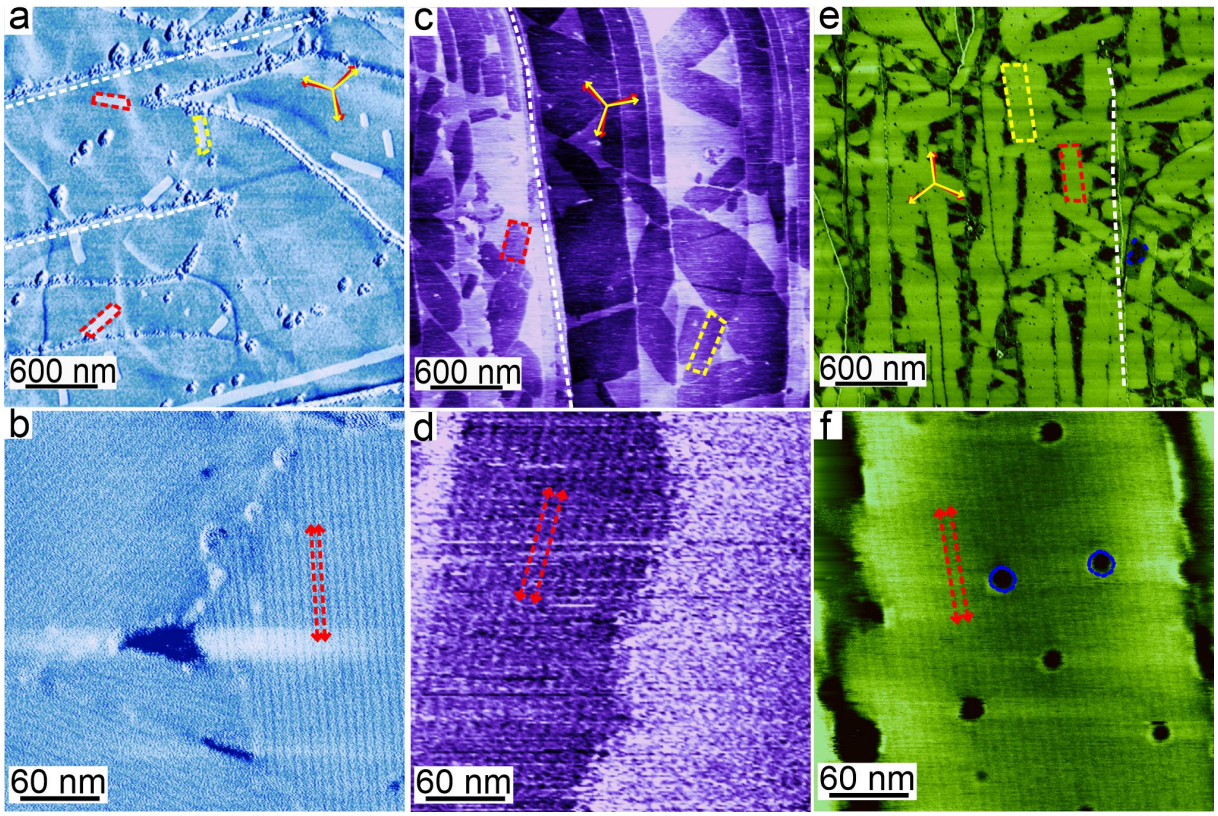

Figure 5: Additional AFM phase images of monolayer film of FcC3 (a,b), FcC3-Pd (c,d) and FcC3-Cu (e,f) on HOPG(0001) surface deposited from methanol at ambient temperature. Molecular islands of FcC3, FcC3-Pd and FcC3-Cu are marked with red and yellow dashed lines. Few graphite step edges are marked with white dashed lines. Red and yellow arrow heads indicate the orientations of molecular islands. Double headed arrows indicate line-like contrast running along the length of molecular islands. Blue dashed line in the film of FcC3-Cu shows additional type of islands.

S6: AFM topographs of monolayer film of FcC5, FcC5-Pd and FcC5-Cu

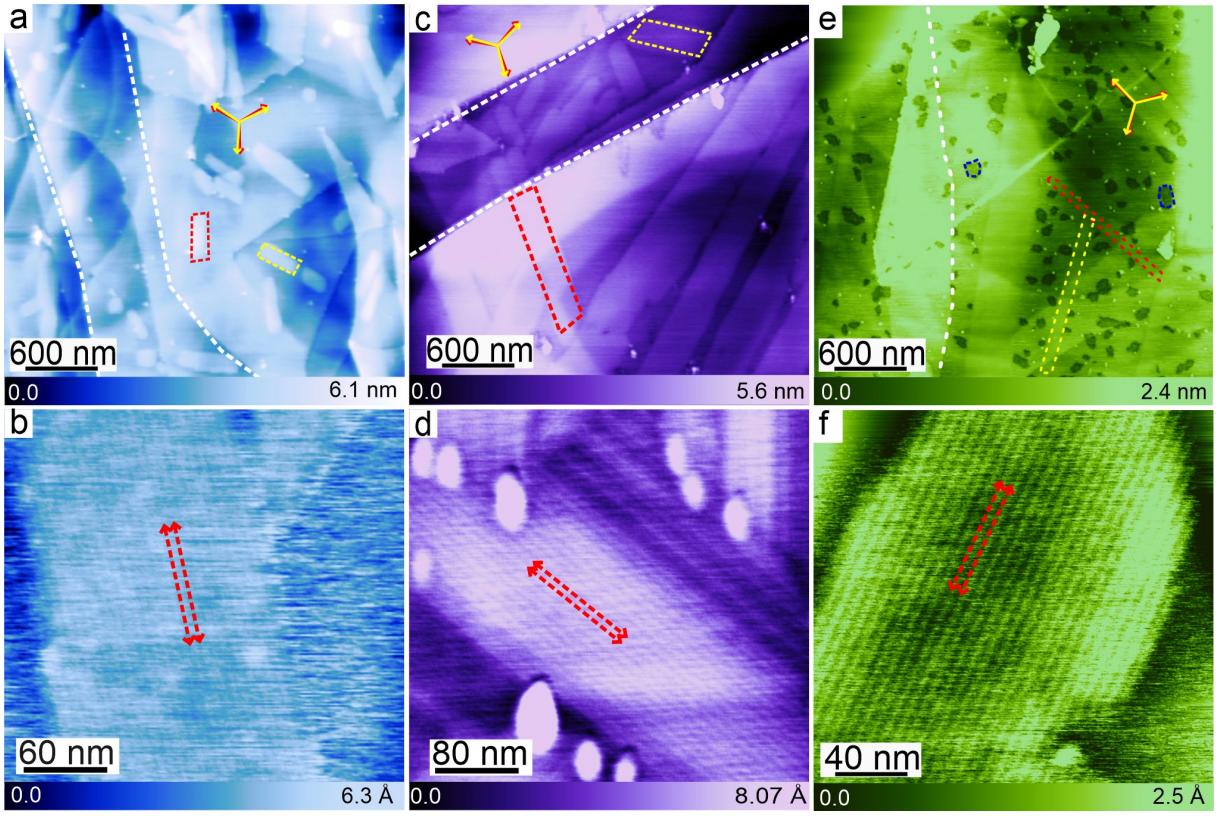

Figure 6: AFM topograph images of monolayer film of FcC5 (a,b), FcC5-Pd (c,d) and FcC5-Cu (e,f) on HOPG(0001) surface deposited from methanol at ambient temperature. The topographs corresponds to the phase images shown in Figure 3 of Manuscript. Molecular islands of FcC5, FcC5-Pd and FcC5-Cu are marked with red and yellow dashed lines. Few graphite step edges are marked with white dashed lines. Red and yellow arrow heads indicate the orientations of molecular islands. Double headed arrows indicate line-like contrast running along the length of molecular islands. Blue dashed line in the film of FcC5-Pd and FcC5-Cu shows additional type of islands.

S7: Additonal AFM phase images of monolayer film of FcC5, FcC5-Pd and FcC5-Cu

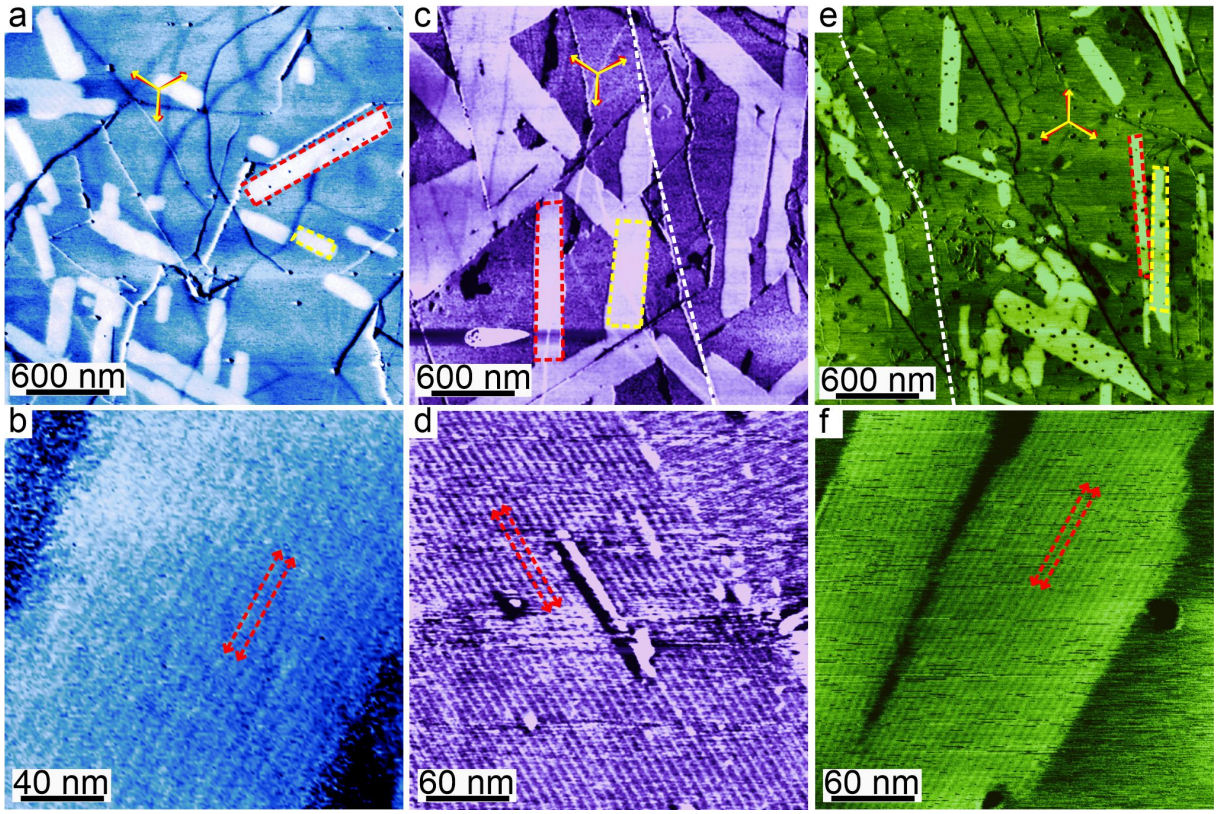

Figure 7: Additional AFM phase images of monolayer film of FcC5 (a,b), FcC5-Pd (c,d) and FcC5-Cu (e,f) on HOPG(0001) surface deposited from methanol at ambient temperature. Molecular islands of FcC5, FcC5-Pd and FcC5-Cu are marked with red and yellow dashed lines. Few graphite step edges are marked with white dashed lines. Red and yellow arrow heads indicate the orientations of molecular islands. Double headed arrows indicate line-like contrast running along the length of molecular islands. Blue dashed line in the film of FcC5-Pd and FcC5-Cu shows additional type of islands.

S8: 2D-FFT of high resolution AFM phase images of monolayer of FcC5, FcC5-Pd and FcC5-Cu

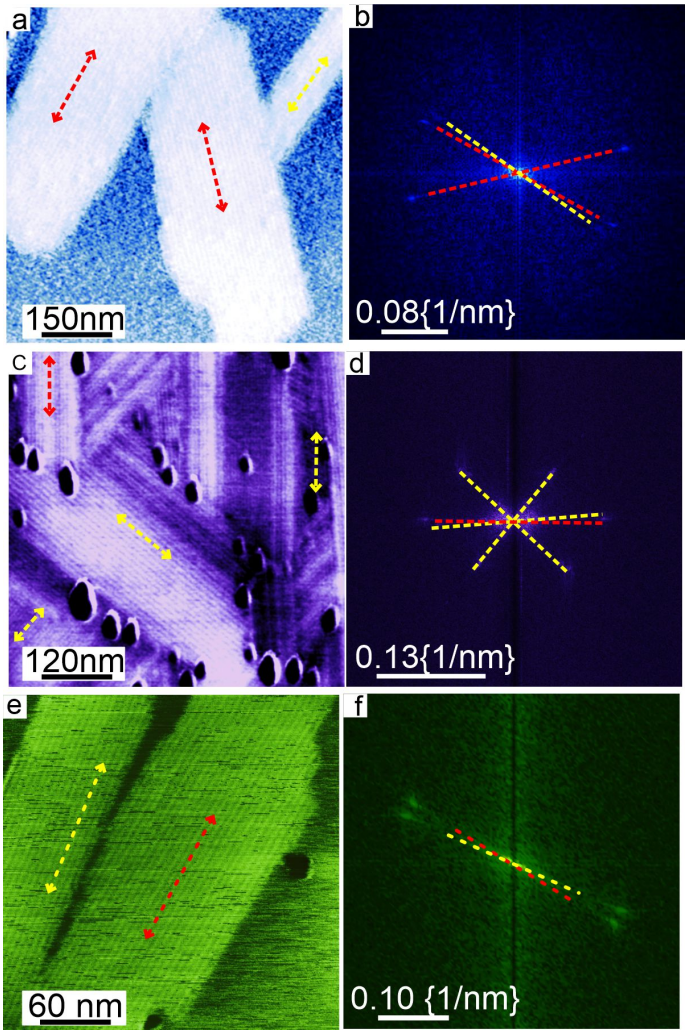

Figure 8: (a) High resolution AFM phase image of monolayer of FcC5 (a), FcC5-Pd (c) and FcC5-Cu (e) on HOPG(0001). The corresponding 2D-FFT of a, c, and e are shown in b, d, and f, respectively.

Molecular islands appear as long well defined islands. Line-like contrast corresponds to the molecular super-lattice. The super-lattice is clearly visible in the 2D-FFT. Red and yellow arrows indicate the orientation of two domains that are mirror image to each other. This mirror image leads to the observation of six orientation for the molecular islands on surface. The mirror domains are oriented by $\approx 12\ ^{\circ}$ with respect to each other. That is,

each molecular domain is rotated by $\approx 6^{\circ}$ with respect to the graphite compact directions. Note that the angles between the mirror domains are approximately same for FcC5 and FcC5-Pd/Cu films.

S9: Pd 3d and Cu 2p XPS spectra of FcC3/FcC5-Cu and FcC3/FcC5-Pd

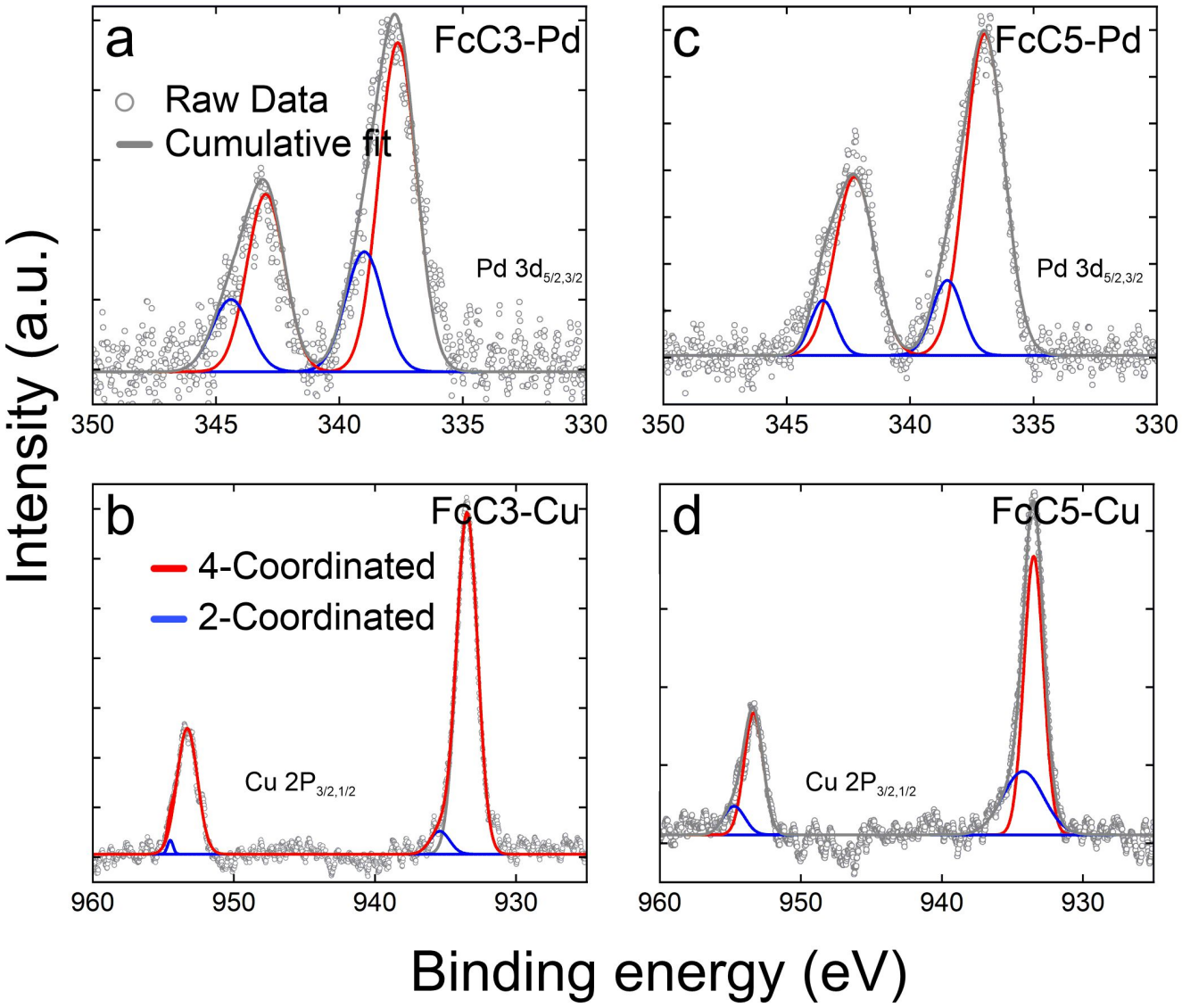

Figure 9: XPS spectra corresponding to $3d_{5/2}$ ($3d_{3/2}$) and $2p_{3/2}$ ($2p_{1/2}$) resonances for FcC3-Pd (a), FcC3-Cu (b), FcC5-Pd (c), and FcC5-Cu (d).

Table 1: Binding Energies and FWHM for $Pd3d_{5/2}$ ($Pd3d_{3/2}$) and $Cu2p_{3/2}$ ($Cu2p_{1/2}$) resonances in FcC3-Pd/Cu and FcC5-Pd/Cu film.

Resonances	$3d_{5/2}$ ($3d_{3/2}$)	$3d_{5/2}$($3d_{3/2}$)	Area ratio*	FWHM (eV)
FcC3-Pd	337.6 (338.9)	342.9 (344.4)	3.3:2	1.79 (1.79)
FcC5 Pd	337.0 (338.5)	342.3 (343.5)	3.2:2	1.88 (1.43)
$PdCl_2$	337.1 (342.4)	342.5 (343.3)	3.2:2	1.82 (1.67)
	$2p_{3/2}$ ($2p_{1/2}$)	$2p_{3/2}$ ($2p_{1/2}$)	Area ratio	FWHM (eV)
FcC3-Cu	933.5 (935.4)	953.3 (954.5)	2:1	1.74 (1.64)
FcC5-Cu	933.5 (934.3)	953.4 (954.7)	2.1:1	1.63 (3.41)
$CuCl_2$	933.2 (934.9)	953.2 (955.3)	2:1	1.71 (1.8)

* Theoretical ratio of area between $3d_{5/2}$ and $3d_{3/2}$ is 3:2 and that of $2p_{3/2}$ and $2p_{1/2}$ is 2:1.

S10: O 1s XPS spectra of FcC3/FcC5, FcC3/FcC5-Cu and FcC3/FcC5-Pd

Table 2: The Binding energy values for C1s and O1s for FcC3, FcC5, FcC3-Pd/Cu and FcC5-Pd/Cu.

Sample	C1s	O1s (1)	O1s (2)
FcC3	284.82	534.32	532.80
FcC5	284.81	534.36	532.70
FcC3-Pd	284.82	535.70	533.10
FcC5-Pd	284.81	534.40	532.80
FcC3-Cu	284.81	534.50	532.80
FcC5-Cu	284.81	535.10	532.60

The major O1s resonance observed in different films of FcC3/FcC5 with and without Cu/Pd are shown in Figure S11; FcC3 (a), FcC5 (d), FcC3-Pd (b), FcC5-Pd (e), FcC3-Cu (c), FcC5-Cu (f). The values of the resonances are listed in Table 2. The major C1s resonances in all cases are around 284.8 eV and it corresponds to sp2 carbon as expected for FcC3/FcC5. The carbon peak is also used for the calibration of other peaks. Two O1s resonances are observed for FcC3 and FcC5, at 532.8 (532.7) eV and it corresponds to a hydrogen bonded C=O/C-O group (or partial double bonded C and O). This indicates that majority of FcC3/FcC5 molecules are forming an ordered assembly mediated by dimeric hydrogen bonding of carboxyl groups.[3–10] This is expected as we have seen large well-ordered crystalline domains of self-assembled FcC3/FcC5 films in AFM images. The minor peak at 534.4 corresponding to C–OH group suggesting small percentage of unordered FcC3/FcC5 on surface. This could be originating due to unordered molecules near the step edges or small unordered clusters in the films of FcC3/FcC5. It is interesting to note that upon Cu or Pd doping of FcC3/FcC5 film, the major O1s peak remains near 532.8 eV. This suggest that the oxygen is bound to the metal.[11–14] The binding energy is comparable to that of –C=O oxygen indicating a weak four coordination of metal to oxygen. The minor peak observed is around 534.5 eV indicating a strongly oxidized oxygen. We presume that this is most

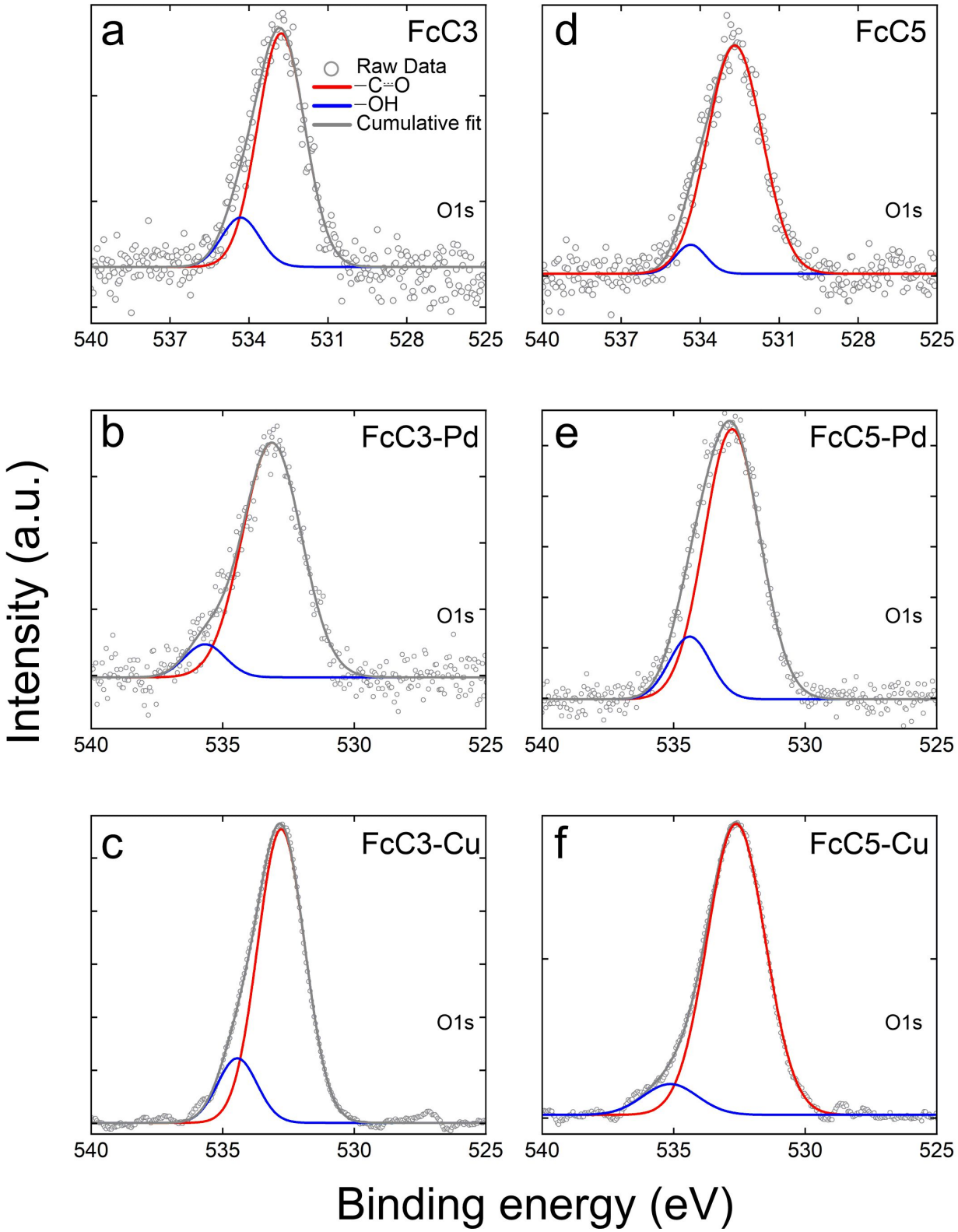

Figure 10: XPS spectra of O1s for FcC3 (a), FcC3-Pd (b), FcC3-Cu (c), FcC5 (d), FcC5-Pd (e), and FcC5-Cu (f).

likely due to 2-coordinated FcC3/FcC5-Pd/Cu, where oxygen is strongly bound to the metal atoms. The calculation of 2 coordinated dimers of FcC3/FcC5-Pd/Cu reveals either shorted metal–oxygen bond length of nonplanarity. This is attributed to the a relaxed geometry of 2 coordinated dimers compared to 4 coordinate dimer, which are more planar. See S15 for details. That is the majority of the metal doped FcC3/FcC5 films is 4-coordinated and a small faction is 2-coordinated. This may also be correlated to the two types of islands observed in the metal coordinated films where majority of the film consists of long islands and small faction of 2D islands.

S11: Hydrogen bonded and Pd/Cu coordinated dimers of FcC3 and FcC5

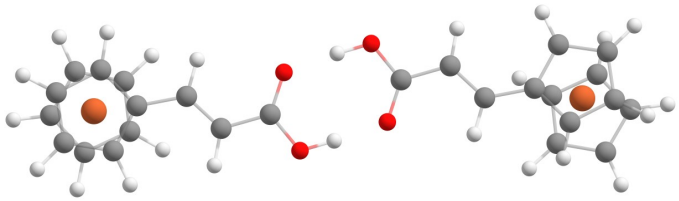

FcC3

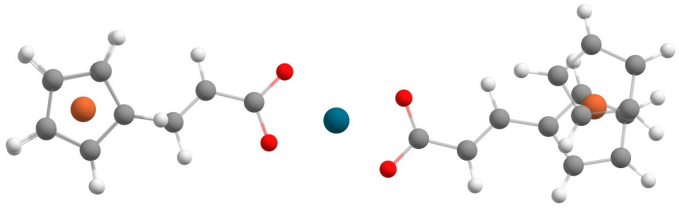

FcC3-Pd**

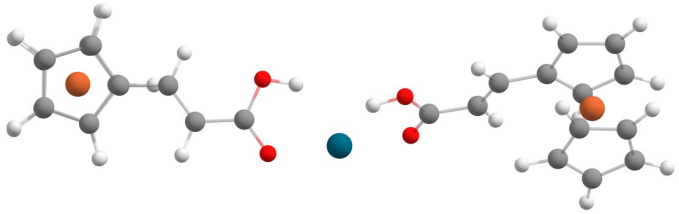

FcC3-Pd*

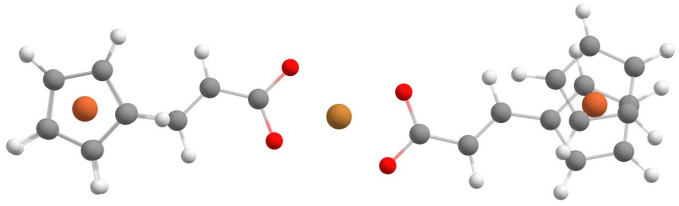

FcC3-Cu**

FcC3-Cu*

Figure 11: Optimized minimum energy geometry of hydrogen bonded and Pd/Cu coordinated dimers of FcC3. * 2-coordinated dimers; ** 4-coordinated dimer.

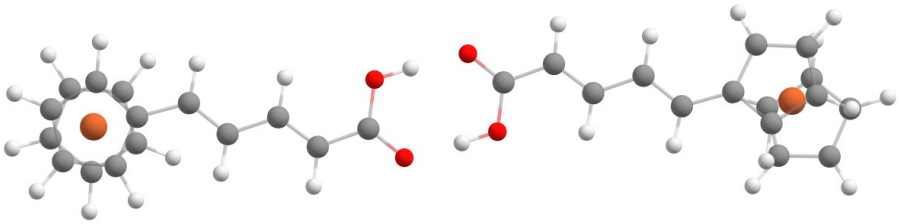

FcC5

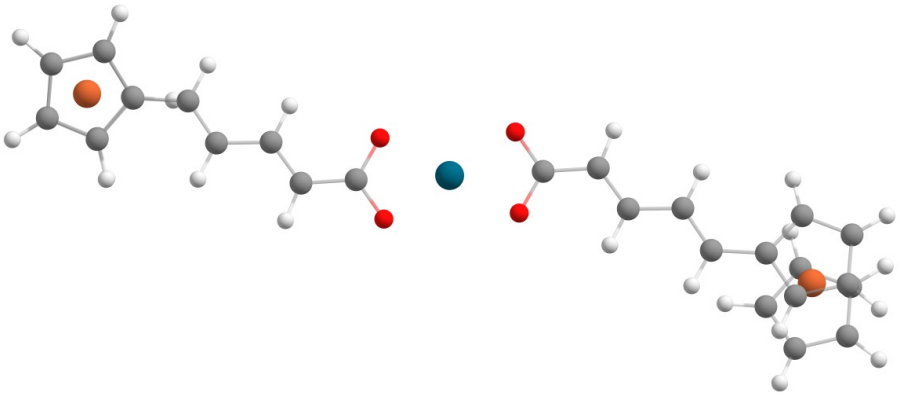

FcC5-Pd**

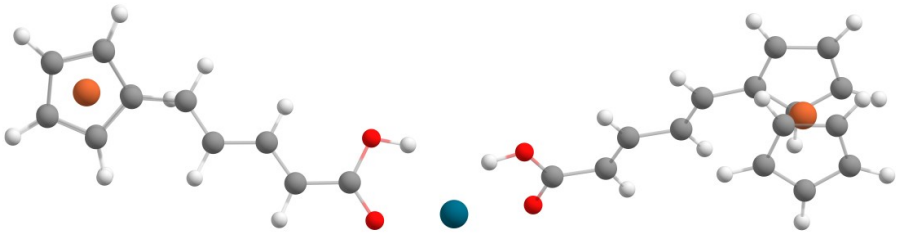

FcC5-Pd*

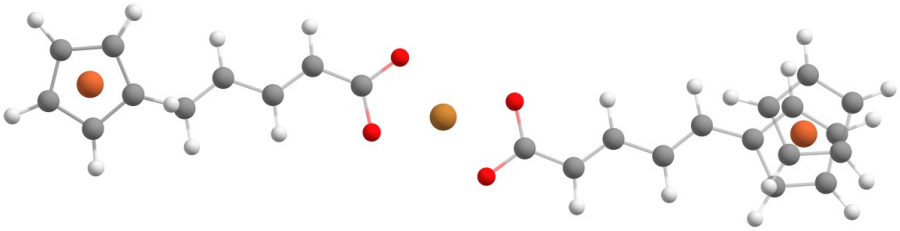

FcC5-Cu**

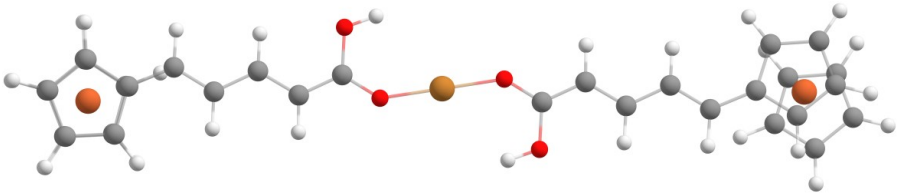

FcC5-Cu*

Figure 12: Optimized minimum energy geometry of hydrogen bonded and Pd/Cu coordinated dimers of FcC5. * 2-coordinated dimers; ** 4-coordinated dimer.

Table 3: Pd–O and Cu–O distances of the optimized dimers of FcC3/FcC5-Pd/Cu

Type	FcC3-Pd(Pd–O)	FcC3-Cu(Cu–O)	FcC5-Pd(Pd–O)	FcC5-Cu(Cu–O)
*	2.10	1.83	2.13	1.84
**	2.09	2.015	2.09	2.015

* 2 coordinated; ** 4 coordinated; all values are in Å.

S12: Dimer based assemblies of FcC3 and FcC3-Cu, FcC5 and FcC5-Pd

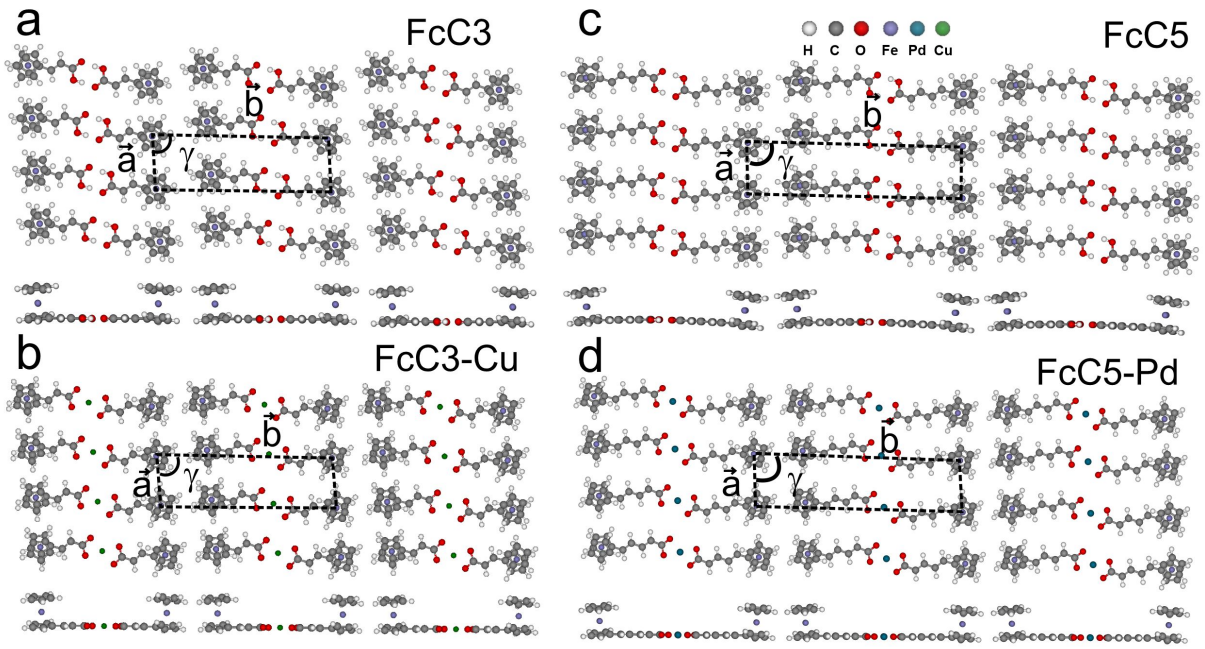

Figure 13: Tentative models for the adlayer of FcC3 (a), FcC3-Cu (b), FcC5 (c) and FcC5-Pd (d). The unit cells are indicated by **a**, **b**, and γ as unit lattice vectors and angle between the vectors. Side view of the model along the lattice direction **a** is shown in the lower panel. The unit cell of FcC3 and FcC3-Cu assembly is depicted by black oblique with the unit cell vectors **a** (0.60 nm), **b** (1.85 ± 0.05 nm) and γ (87 °) the angle between the vectors. Similarly, the unit cell of FcC5 and FcC5-Pd assembly is depicted by black oblique with the unit cell vectors **a** (0.65 nm), **b** (2.35 ± 0.05 nm) and γ (87 °) the angle between the vectors.

S13: STM analysis of FcC3 and FcC5 monolayer films on HOPG

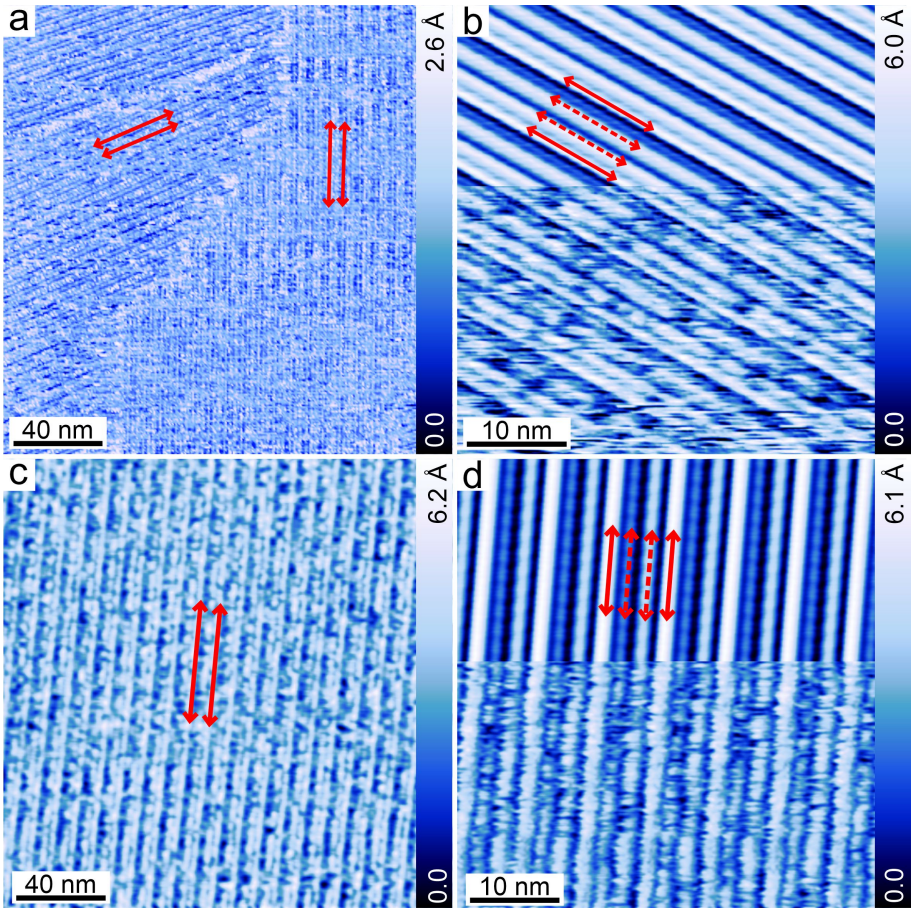

Figure 14: (a, c) Constant current STM topography (V = 0.5 V, I = 300 pA) of the adlayer of FcC3 and FcC5 on HOPG (0001) imaged at air interface. The red solid double headed arrows indicate a super-lattice. (b, d) High resolution STM topographs of FcC3 and FcC5 along with the mesh averaged image (top panel).

To understand the microscopic arrangement of molecules in the film, we have employed STM measurements. Constant current STM topography of monolayer films of FcC3 adlayer on HOPG (0001) are shown in Figure 14a. Different domains oriented by ≈ 60 ° are also observed. A high-resolution STM topography of part of a molecular island of FcC3 is shown in Figure 14b with upper half an averaged image. The solid red double headed arrows indicate bright line-like contrasts originating from a super-periodic lattice. The spac-

ing between these bright line-like contrasts is 6.1 ± 0.3 nm and it correlates well with the super-periodicity observed in the molecular islands with AFM. High resolution image further reveals more line-like features corresponding to adjacent molecular lattices and are marked by dashed red double headed arrows (Figure 14a). The average distance between the adjacent line-like contrasts (between solid/dashed double headed arrows) are spaced by 1.9 ± 0.1 nm and the spacing corresponds to the length of an optimized FcC3 dimer. The longest axis through carboxyl group of FcC3 dimer is 1.85 nm (cf. S11). Similarly, constant current STM topograph of monolayer films of FcC5 adlayers on HOPG (0001) are shown in Figure 14c. A high-resolution STM topography of a part of a molecular island of FcC5 is shown in Figure 14d with upper half an averaged image. The solid red double headed arrows indicate bright line-like contrasts originating from a super-periodic lattice. The spacing between these bright line-like contrasts is 7.0 ± 0.2 nm, which correlates well with the super-periodicity observed in the molecular islands with AFM. High resolution image further reveals more line-like features corresponding to adjacent molecular lattice and are marked by dashed red double headed arrows. The average distance between the adjacent line-like contrasts (between solid/dashed double headed arrows) is spaced by 2.4 ± 0.1 nm and the spacing corresponds to the length of the optimized FcC5 dimer. The longest axis through carboxyl group is 2.38 nm (cf. S11). Thus, we tentatively attribute that the line-like contrast in both FcC3 and FcC5 are originating from the dimer based molecular lattice.

S14: STM analysis of FcC3-Pd monolayer films on HOPG

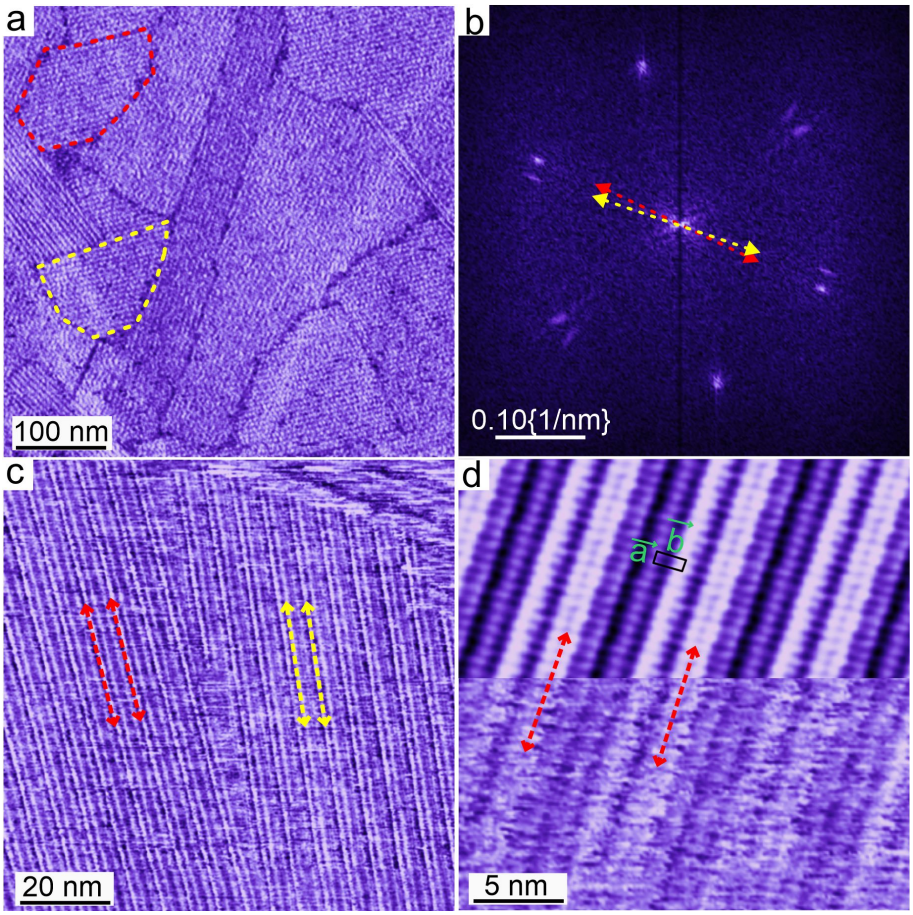

Figure 15: Constant current STM topography (V = 0.5 V, I = 300 pA) of the adlayer of FcC3-Pd a HOPG (0001) (a,c). (b) 2D-FFT taken on the image produced in a. (d) High resolution STM topographs (V = 0.5 V, I = 300 pA) of FcC3-Pd along with the mesh averaged image (top panel). Red and yellow double headed arrows indicate the orientation of two domains that are mirror image to each other.

The mirror image leads to the observation of six orientation for the molecular islands on surface. The mirror domains are oriented by $\approx 6\,^{\circ}$ with respect to each other. That is each molecular domain is rotated by $\approx 3\,^{\circ}$ with respect to the graphite compact directions. The orientation is matching with the observations obtained in the AFM images of films of FcC3-Pd. The high-resolution image reveals a nearly rectangular unit cell (marked with black rectangle) for the monolayer of FcC3-Pd. The unit cell parameters as follows, **b** ($1.85 \pm 0.05\,\mathrm{nm}$), **a** ($1.03 \pm 0.02\,\mathrm{nm}$) and γ ($87\,^{\circ}$) the angle between the vectors.

S15: Multiple I-V curves used for the averaging in FcC3 and FcC5.

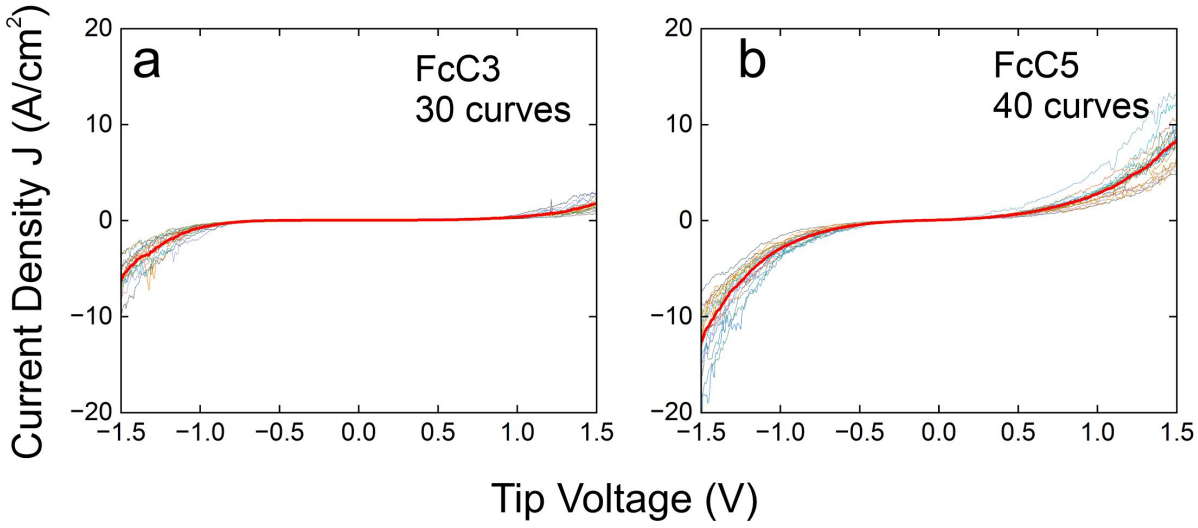

Figure 16: I-V curves used for the averaging the I-V of FcC3 and FcC5 films.

S16: Multiple I-V curves used for the averaging of FcC3-Pd and FcC3-Cu films.

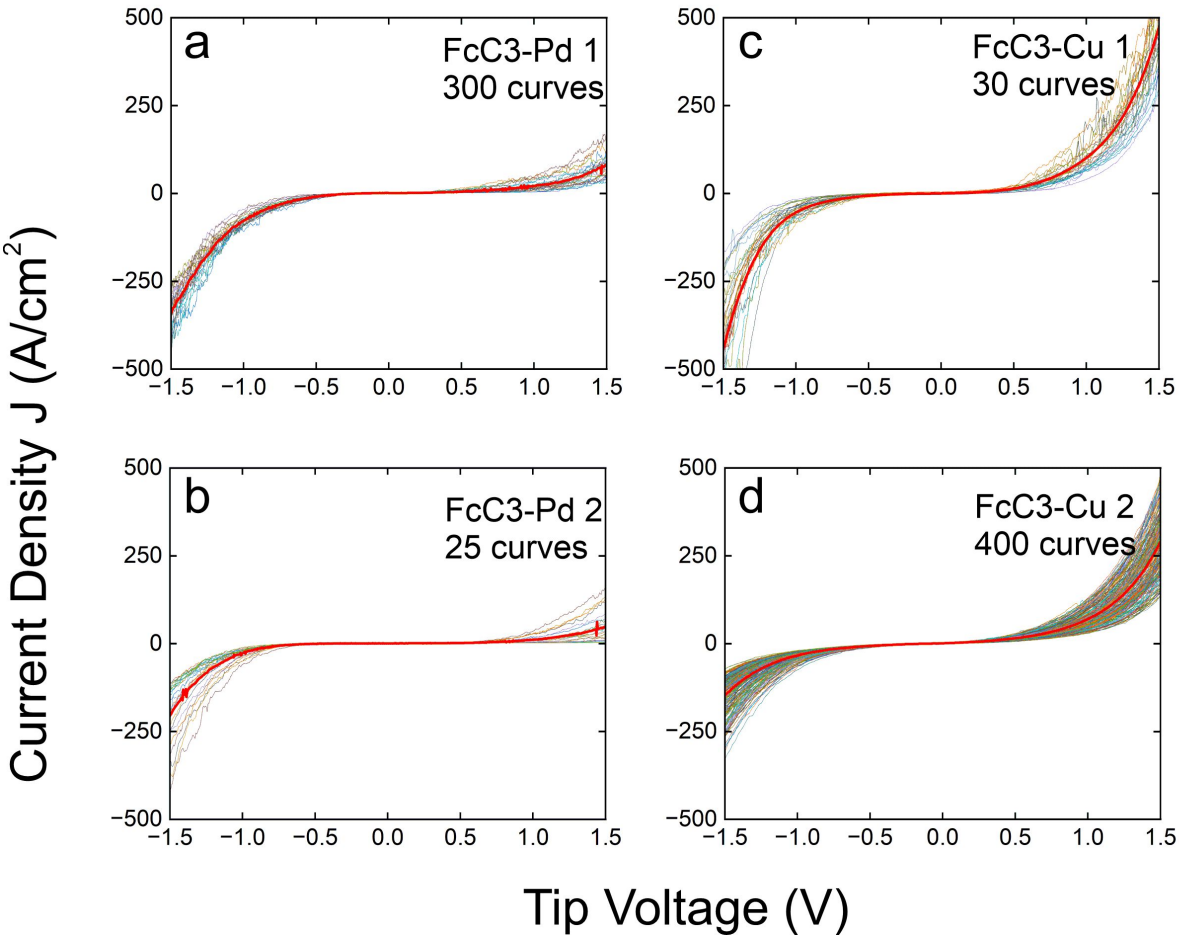

Figure 17: Multiple I-V curves used for the averaging I-V of FcC3-Pd and FcC3-Cu films. The indexes 1 and 2 correspond to two different set of data.

S17: Multiple I-V curves used for the averaging of FcC5-Pd and FcC5-Cu films.

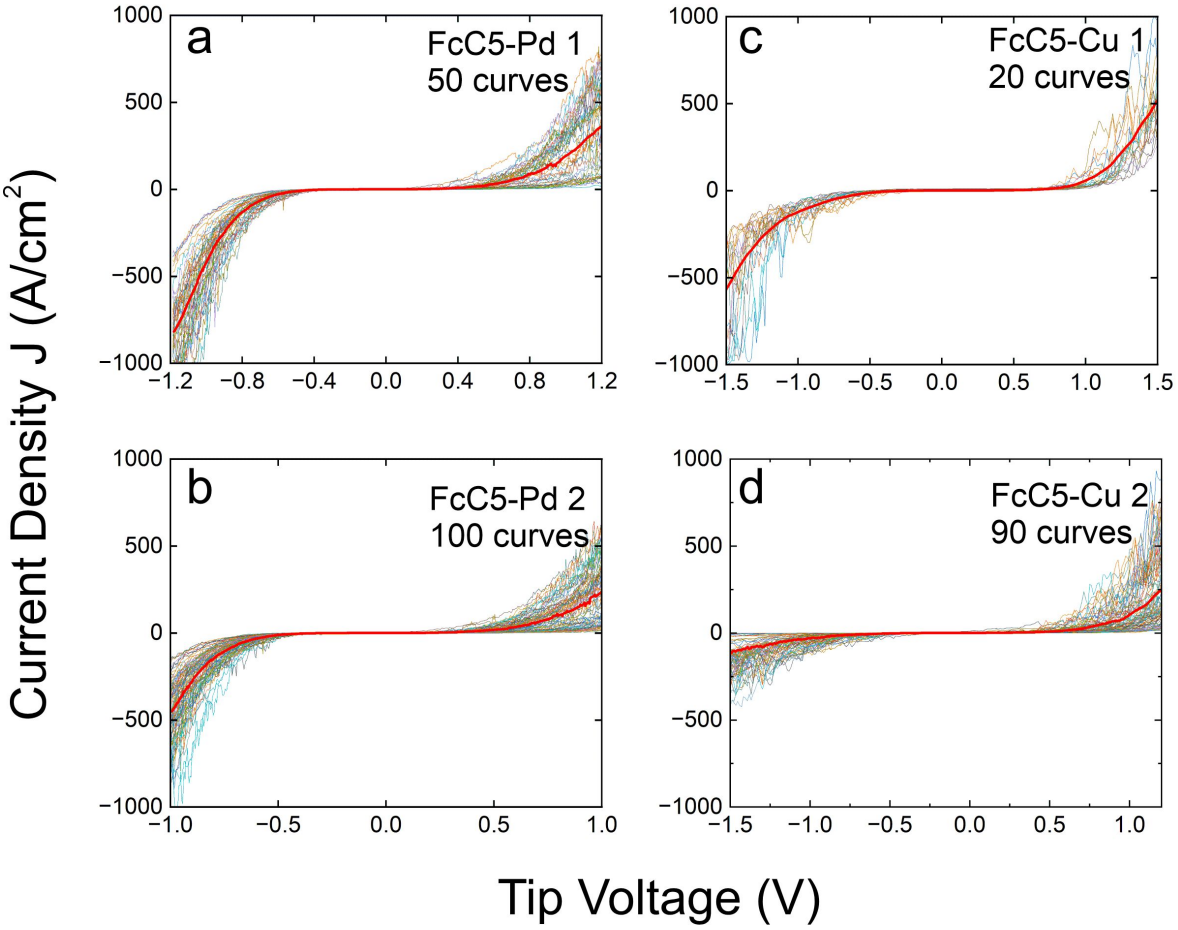

Figure 18: Multiple I-V curves used for the averaging I-V of FcC5-Pd and FcC5-Cu film. The indexes 1 and 2 correspond to two different set of data.

S18: Comparison of averaged I-V curve of monolayer films of FcC3 and FcC5.

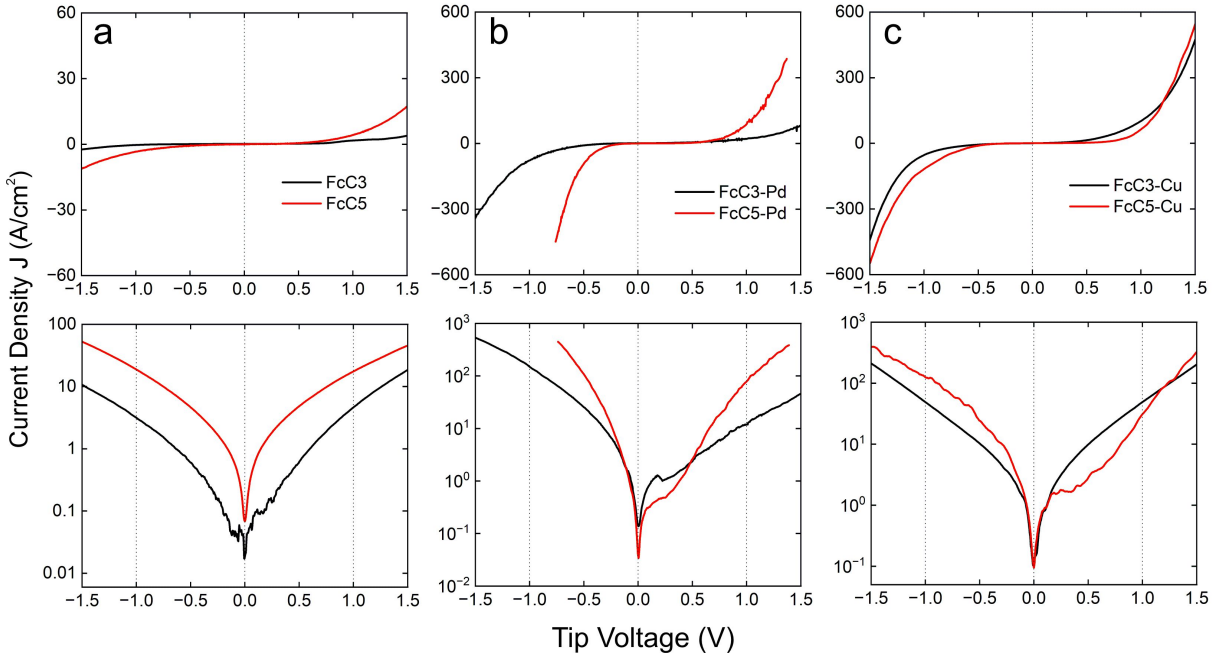

Figure 19: Comparison of average I-V curves of FcC3 and FcC5 (a), FcC3-Pd and FcC5-Pd (b) and FcC3-Cu and FcC5-Cu (c). Black and red lines represent FcC3 and FcC5, respectively. The conductivity of FcC5 film is higher than that of FcC3 film. The calculations and V^2/I vs V plot reveals that the HOMO-LUMO gap of FcC5 is smaller than that of FcC3. A reduced HOMO-LUMO gap is expected for FcC5 dimers as it has longer conjugated double bonds compared to FcC3 dimers. So we attribute that the increased conductivity is due to the smaller HOMO-LUMO gap. While there is a significant difference in the conductivity obtained on Pd doped FcC3 and FcC5 films, the Cu doped films of both FcC3 and FcC5 are comparable, comparison made at -1 V and +1 V.

S19: Plot of V^2/I vs tip voltage V

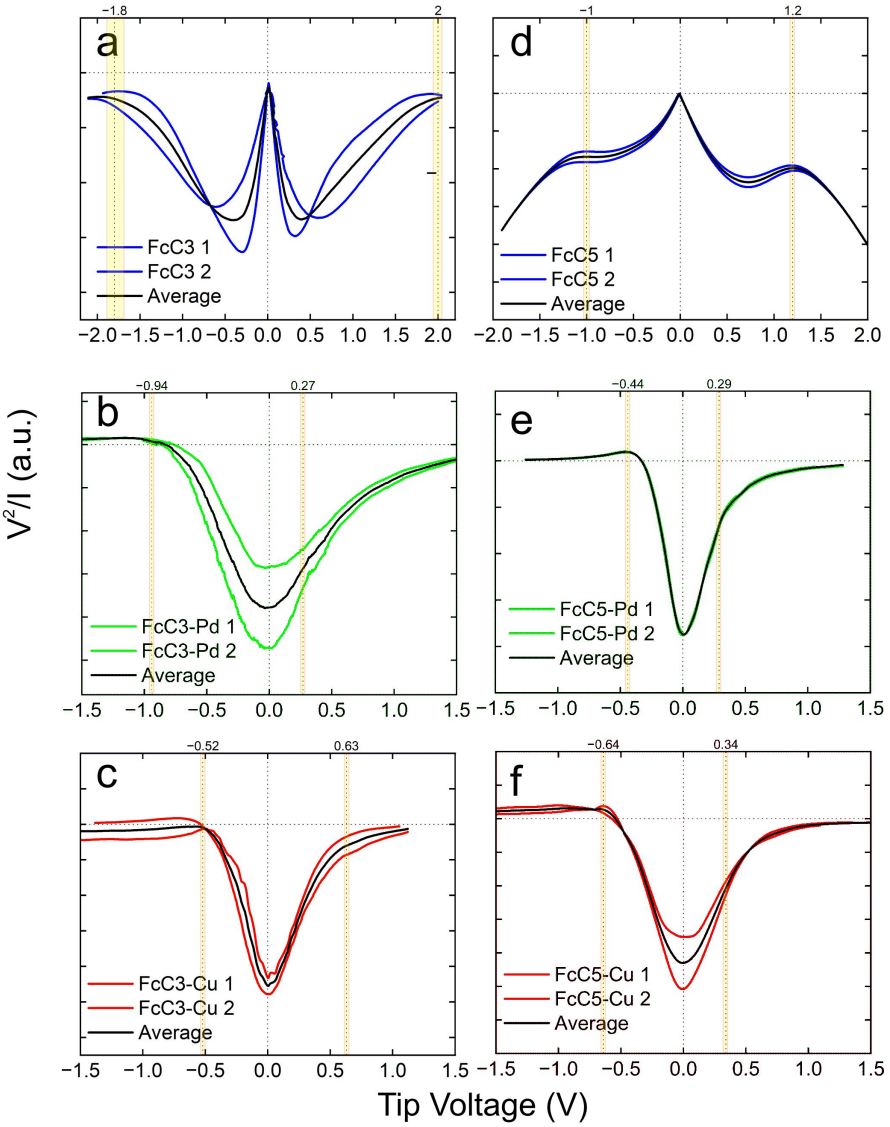

Figure 20: Plot of V^2/I vs tip voltage V for FcC3 (a), FcC5 (d), FcC3-Pd (b), FcC5-Pd (e), FcC3-Cu (c), FcC5-Cu (f). Average of two set of data is shown and the average of these sets are given as black curve. Light yellow band in the figures corresponds to the position of the HOMO and LUMO.

Since voltage is applied with respect to the tip, the negative bias corresponds to unfilled and positive bias corresponds to filled orbitals. The voltage corresponds to the change in the V^2/I value at the $V_{\max}$ position after the first-order derivative of the function V^2/I is used to determine the HOMO/LUMO positions as per literature.[15,16] To find the position

of HOMO and LUMO (ϵ_h), the maxima of V^2/I is equated to zero and ϵ_h is extracted as follows,

$$\epsilon_h = \frac{\sqrt{3}e|V_t|}{2}$$

where V_t is the maximum transition voltage for the junction. The position of the HOMO and LUMO extracted are provided in Table 4. For cases where a maxima is not observed in the V^2/I, we used $ln(J)$ vs V. Due to presence of localized electronic states (in our case HOMO/LUMO), sharp variations are expected in $ln(J)$ vs V.[15,16] Such variations, due to the involvement of orbital mediated transport, are indicated using arrow heads in Figure 5c and 5d of the main manuscript. The conductivity near zero voltage (G) due to the background tunneling[16] for all cases are provided in Table 4. G is comparable in all cases. This is attributed due to the fact that the layer thickness is comparable (one layer) and therefore the background tunneling to be comparable. However, we note that the overall G of metal doped films is higher than that for FcC3/FcC5. We attribute this to be related to the reduced barrier for electron tunneling in the metal doped FcC3/FcC5.

Table 4: HOMO and LUMO energies of different molecular films obtained from V^2/I vs tip voltage V and I vs V plots. Low bias conductance (G) obtained from the I-V curves on different molecular films.

.	FcC3	FcC3-Pd	FcC3-Cu	FcC5	FcC5-Pd	FcC5-Cu
HOMO (eV)	-1.56	-0.81	-0.45	-0.87	-0.38	-0.55
LUMO (eV)	1.73	0.23	0.55	1.04	0.25	0.29
G (nS)	0.03	0.32	0.43	0.15	0.30	0.23

S20: Details of theoretical calculations

Table 5: Theoretically obtained HOMO and LUMO energies of different dimers.

Theotical	FcC3	FcC3-Pd	FcC3-Cu	FcC5	FcC5-Pd	FcC5-Cu
HOMO**	-5.57	-5.94	-5.84	-5.68	-5.84	-5.74
LUMO**	-1.83	-3.08	-3.44	-2.22	3.01	-3.35
HOMO*	-5.57	-4.25	-3.37	-5.68	-4.23	-3.48
LUMO*	-1.83	-2.56	-2.84	-2.22	-2.79	-3.03

* 2 coordinated; ** 4 coordinated; all values are in (eV)

References

(1) Galangau, O.; Dumas-Verdes, C.; Schmidt, E. Y.; Trofimov, B. A.; Clavier, G. N-Vinyl Ferrocenophane Pyrrole: Synthesis and Physical and Chemical Properties. *Organometallics* **2011**, *30*, 6476–6481.

(2) Inamura, S.; Fujimoto, Y.; Kawasaki, A.; Shiokawa, Z.; Woelk, E.; Heine, H.; Lindner, B.; Inohara, N.; Kusumoto, S.; Fukase, K. Synthesis of peptidoglycan fragments and evaluation of their biological activity. *Org. Biomol. Chem.* **2006**, *4*, 232–242.

(3) Tait, S. L.; Wang, Y.; Costantini, G.; Lin, N.; Baraldi, A.; Esch, F.; Petaccia, L.; Lizzit, S.; Kern, K. Metal–Organic Coordination Interactions in Fe–Terephthalic Acid Networks on Cu(100). *J. Am. Chem. Soc.* **2008**, *130*, 2108–2113.

(4) Stepanow, S.; Ohmann, R.; Leroy, F.; Lin, N.; Strunskus, T.; Wöll, C.; Kern, K. Rational Design of Two-Dimensional Nanoscale Networks by Electrostatic Interactions at Surfaces. *ACS Nano* **2010**, *4*, 1813–1820.

(5) Ruben, M.; Lehn, J.-M.; Müller, P. Addressing metal centres in supramolecular assemblies. *Chem. Soc. Rev.* **2006**, *35*, 1056–1067.

(6) Chen, Q.; Perry, C.; Frederick, B.; Murray, P.; Haq, S.; Richardson, N. Structural aspects of the low-temperature deprotonation of benzoic acid on Cu(110) surfaces. *Surf. Sci.* **2000**, *446*, 63–75.

(7) Auwärter, W.; Weber-Bargioni, A.; Brink, S.; Riemann, A.; Schiffrin, A.; Ruben, M.; Barth, J. V. Controlled Metalation of Self-Assembled Porphyrin Nanoarrays in Two Dimensions. *Chem. Phys. Chem.* **2007**, *8*, 250–254.

(8) Shubina, T. E.; Marbach, H.; Flechtner, K.; Kretschmann, A.; Jux, N.; Buchner, F.; Steinrück, H.-P.; Clark, T.; Gottfried, J. M. Principle and Mechanism of Direct Por-

phyrin Metalation: Joint Experimental and Theoretical Investigation. *J. Am. Chem. Soc.* **2007**, *129*, 9476–9483.

(9) Messina, P.; Dmitriev, A.; Lin, N.; Spillmann, H.; Abel, M.; Barth, J. V.; Kern, K. Direct Observation of Chiral Metal-Organic Complexes Assembled on a Cu(100) Surface. *J. Am. Chem. Soc.* **2002**, *124*, 14000–14001.

(10) Lin, T.; Kuang, G.; Shang, X. S.; Liu, P. N.; Lin, N. Self-assembly of metal-organic coordination networks using on-surface synthesized ligands. *Chem. Commun.* **2014**, *50*, 15327–15329.

(11) Mishra, V.; Mir, S. H.; Singh, J. K.; Gopakumar, T. G. Rationally Designed Semiconducting 2D Surface-Confined Metal-Organic Network. *ACS Appl. Mater. Interfaces* **2020**, *12*, 51122–51132.

(12) Nagai, H.; Sato, M. In *Modern Technologies for Creating the Thin-film Systems and Coatings*; Nikitenkov, N. N., Ed.; IntechOpen: Rijeka, 2017; Chapter 1.

(13) Urbán, B.; Papp, M.; Srankó, D.; Skoda-Földes, R. Phosphine-free Atmospheric Carbonylation of Aryl Iodides with Aniline Derivatives in the Presence of a Reusable Silica-supported Palladium Catalyst. *J. Mol. Catal. A Chem.* **2015**, *397*, 150–157.

(14) Ivanova, T.; Maslakov, K.; Sidorov, A.; Kiskin, M.; Linko, R.; Savilov, S.; Lunin, V.; Eremenko, I. XPS detection of unusual Cu(II) to Cu(I) transition on the surface of complexes with redox-active ligands. *J. Electron Spectrosc. Relat. Phenom.* **2020**, *238*, 146878.

(15) Bâldea, I.; Xie, Z.; Frisbie, C. D. Uncovering a law of corresponding states for electron tunneling in molecular junctions. *Nanoscale* **2015**, *7*, 10465–10471.

(16) Nguyen, Q. V.; Xie, Z.; Frisbie, C. D. Quantifying Molecular Structure-Tunneling

Conductance Relationships: Oligophenylene Dimethanethiol vs Oligophenylene Dithiol Molecular Junctions. *J. Phys. Chem. C* **2021**, *125*, 4292–4298.